Progress In Electromagnetics Research, Vol. 116, 381–393, 2011

A NOVEL STRATEGY FOR TOPSIDE IONOSPHERE SOUNDER BASED ON SPACEBORNE MIMO RADAR WITH FDCD

J. Chen*, Z. Li, and C. S. Li

School of Electronics and Information Engineering, Beihang University, Beijing 100191, China

Abstract—A novel strategy for topside ionosphere sounder based on spaceborne Multiple-Input Multiple-Output (MIMO) radar is proposed, which takes advantage of frequency division and code division (FDCD) as a substitution for swept-frequency regime employed by the current ionosphere explorers, e.g., TOPside Automated Sounder (TOPAS). The azimuth resolution can be improved by 153 times compared with TOPAS by means of frequency division, producing two-dimensional electron density images. The signal-to-noise ratio (SNR) can be enhanced and complete orthogonality among channels at different frequencies can be achieved by code division, which uses Complete Complementary Sequence (CCS) as phase coding waveform. The simulation results show that root mean square (RMS) of normalized electron density measurements error of novel ionosphere sounder is as low as 1.7%.

1. INTRODUCTION

Ionosphere is an essential constituent of Earth's space weather system, which has significant impacts on electromagnetic (EM) wave propagation [1–3]. The topside ionosphere is the region above F2 layer in ionosphere, and the topside ionosphere exploration is of great importance for space information systems, e.g., satellite communication, navigation and remote sensing etc. [4]. Current spaceborne topside explorers, e.g., TOPAS (TOPside Automated Sounder), play an important role in observing topside electron density distribution at global scale, by transmitting swept-frequency pulses and

Received 11 March 2011, Accepted 6 May 2011, Scheduled 11 May 2011

* Corresponding author: Jie Chen (chenjie@buaa.edu.cn).

measuring delay time of the radar echoes to generate one-dimensional electron density profiles [4]. However, such systems have poor azimuth resolution for employing swept-frequency regime, e.g., the apparent azimuth resolution of TOPAS is as low as 75 km, corresponding to its swept-frequency duration of 10 s [5].

The conception of MIMO (Multiple-Input Multiple-Output) technique [6–10] led to the development of MIMO radar [11–14] that simultaneously transmits multiple waveforms and receives echo signals through multiple channels. In this study, a novel strategy for topside ionosphere sounder by employing advantage of MIMO radar with frequency division and code division (FDCD) is proposed. An introduction to the principle of ionosphere sounding is given in Section 2. After discussing the proposed scheme in Section 3, the system parameters are designed in Section 4. Finally the proposed system is validated through simulation in Section 5.

2. PRINCIPLE OF TOPSIDE IONOSPHERE SOUNDING

Topside ionosphere sounding is based on the ionosphere reflection of high frequency (HF) band signals transmitted by spaceborne radar. When an 'ordinary' HF band EM wave vertically propagates in ionosphere, collision and magnetic field terms are negligible in Appleton formula [15, 16]. The refractive index of ionosphere is $n = \sqrt{1 - f_p^2/f^2}$, where f_p stands for the plasma frequency corresponding to the electron density $N_e = (f_p/9)^2$, and f denotes EM wave frequency. A signal at frequency f will be reflected at the height where $n = 0$ (corresponding to $f = f_p$) [5], and local electron density equals to $(f/9)^2$.

Assume a spaceborne nadir-looking ionosphere sounding MIMO radar simultaneously transmits multiple signals at different frequencies $f_i (i = 1, \ldots, N)$, which will be reflected at different heights h_i, where the local electron densities $N_e = (f_i/9)^2$. In topside ionosphere, the electron density increases with the decrease of height and the lower boundary of topside ionosphere have the maximum electron density corresponding to maximum plasma frequency f_m. The signals at frequencies smaller than f_m can be reflected and received by the radar. Figure 1 illustrates the schematic of topside ionosphere sounding. In Figure 1(a), the signals at different frequencies, e.g., f_1, f_2, f_{m1}, f_{m2} ($f_1 < f_2 < f_{m1} < f_{m2}$) are reflected at different height. x_1 and x_2 denote two azimuth positions of the satellite with the different maximum plasma frequencies f_{m1} and f_{m2} due to ionospheric disturbance caused by an irregular bubble structure [17] (see (15)–(18)

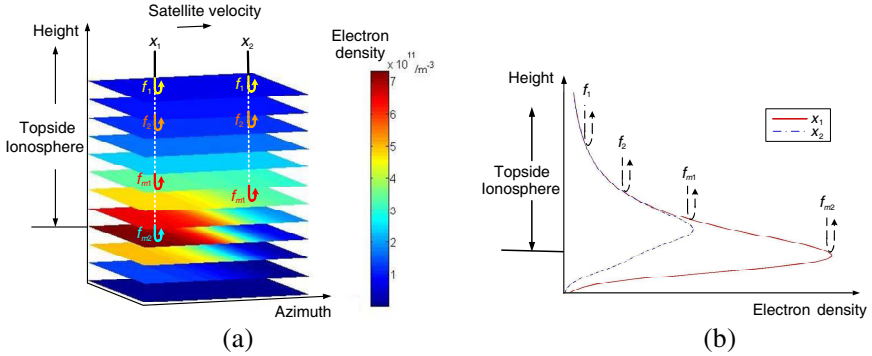

Figure 1. Topside ionosphere sounding schematic diagram. (a) Three-dimensional electron density profile view. (b) One-dimensional electron density profile view at x_1 and x_2.

in Section 5).

Measuring the corresponding delay time t_i of the echo signal at frequency f_i to derive the virtual ranges $\hat{r}_i = c \cdot t_i/2$, where c is light speed in vacuum. The vertical electron density profile can be derived by using the traditional inversion algorithms, e.g., the least-squares polynomial fit algorithm [18].

The virtual range corresponding to frequency f_i is given by

$$\hat{r}_i = \frac{c \cdot t_i}{2} = \frac{c}{2} \cdot 2 \int_0^{r_i} \frac{dr}{v_g} = \int_0^{r_i} n_g dr \tag{1}$$

where $r_i = H_s - h_i$, H_s is satellite height, h_i denotes the true height where the reflection occurs, v_g is the group velocity of the signal, and n_g is the group refractive index of ionosphere given as follows

$$n_g = \frac{\partial(n \cdot f_i)}{\partial f_i} = \frac{f_i}{\sqrt{f_i^2 - f_p^2}} \tag{2}$$

where $n = \sqrt{1 - f_p^2/f^2}$. Putting (2) in (1), the virtual range becomes

$$\hat{r}_i = \int_0^{r_i} \frac{f_i}{\sqrt{f_i^2 - f_p^2}} dr \tag{3}$$

Assume that the true range r as function of the plasma frequency can be given by following polynomial expansion:

$$r = \sum_{k=1}^{M} \alpha_k (f_p - f_v)^k \tag{4}$$

where α_k denote the polynomial coefficients and f_v is the plasma frequency at the satellite height. Hence, (3) can be written as

$$\hat{r}_i = \alpha_k \sum_{k=1}^{M} \int_{f_v}^{f_i} k \frac{f_i (f_p - f_v)^{k-1}}{\sqrt{f_i^2 - f_p^2}} df_p = \sum_{k=1}^{M} \alpha_k \beta_{ik} \tag{5}$$

where

$$\beta_{ik} = \int_{f_v}^{f_i} k \frac{f_i (f_p - f_v)^{k-1}}{\sqrt{f_i^2 - f_p^2}} df_p \tag{6}$$

The N virtual ranges can be expressed by following matrix notation:

$$\hat{\mathbf{r}} = \mathbf{B}\mathbf{a} \tag{7}$$

where α_k, β_{ik}, $\hat{r}_i$ are the elements of $\mathbf{a}$, $\mathbf{B}$, $\hat{\mathbf{r}}$ respectively. $\mathbf{a}$ is $M \times 1$ matrix, $\mathbf{B}$ is $N \times M$ matrix, and $\hat{\mathbf{r}}$ is $N \times 1$ matrix.

For $N > M$, (7) has the least-squares solution:

$$\mathbf{a} = \left(\mathbf{B}^T \mathbf{B}\right)^{-1} \mathbf{B}^T \hat{\mathbf{r}} \tag{8}$$

where $\mathbf{B}^T$ is the transpose of $\mathbf{B}$.

Putting $f_p = 9\sqrt{N_e}$ and $r = H_s - h$ in (4), the electron density N_e as function of height h can be derived.

3. MIMO IONOSPHERE SOUNDER

Assume a MIMO radar system is onboard the satellite, employing N transmitting channels for simultaneously generating radar pulses and N receiving channels for processing echo signals. Each transmitting channel generates signal with different carrier frequency and phase coding, to acquire high azimuth resolution by means of frequency division (FD), and high signal-to-noise ratio (SNR) and complete orthogonality among channels of different frequencies by code division (CD).

N individual frequencies, $f_1, f_2, \ldots, f_N$, are selected with uniform frequency interval $\Delta = (f_{\max} - f_{\min})/(N-1)\,\mathrm{MHz}$, where $f_{\min}$ and $f_{\max}$ denote the minimum and maximum transmitting frequency, respectively. Moreover, the Complete Complementary Sequence (CC-S), a phase coding signal waveform, is selected for transmitting pulses, which has high compression gain and complete orthogonality [19, 20]. N pairs of different CC-Ss are employed, namely $\{A_i, B_i\}$, $i = 1 \ldots N$.

The definition of N pairs of CC-Ss $\{A_i, B_i\}$ is given by [20]:

$$\begin{cases} A_i = (a_i^0, a_i^1, \ldots, a_i^{L-1}) \\ B_i = (b_i^0, b_i^1, \ldots, b_i^{L-1}) \end{cases} \quad i = 1, 2, \ldots, N \tag{9}$$

where a_i and b_i denote the sub-pulse codes taking value from $\{1, -1, j, -j\}$, $j^2 = -1$; and L is the length of A_i and B_i.

$\{A_i, B_i\}$ can be generated using the method given in [21], which satisfies complete orthogonality as [19, 20]:

$$R_{A_iA_i}(\tau) + R_{B_iB_i}(\tau) = \begin{cases} 2L & \tau = 0 \\ 0 & \tau = \pm 1, \pm 2, \ldots, \pm(L-1) \end{cases} \quad i = 1, 2, \ldots, N \tag{10}$$

$$R_{A_iA_j}(\tau) + R_{B_iB_j}(\tau) = 0 \quad \tau = 0, \pm 1, \pm 2, \ldots, \pm(L-1) \quad i = 1, 2, \ldots, N,\ j = 1, 2, \ldots, N,\ i \neq j \tag{11}$$

where $R_{A_iA_j}(\tau)$ and $R_{B_iB_j}(\tau)$ denote the aperiodic correlation functions between A_i and A_j, B_i and B_j respectively. When $i = j$, $R_{A_iA_i}(\tau)$ and $R_{B_iB_i}(\tau)$ is matched filtering of A_i and B_i. (10) is the pulse compression process including matched filtering and addition of $R_{A_iA_i}(\tau)$ and $R_{B_iB_i}(\tau)$. It can be seen that the signal intensity can be enlarged by $2L$ times, leading to improved SNR by $10\log_{10}(2L)$ dB.

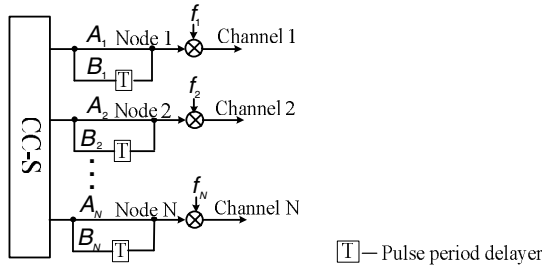

(a)

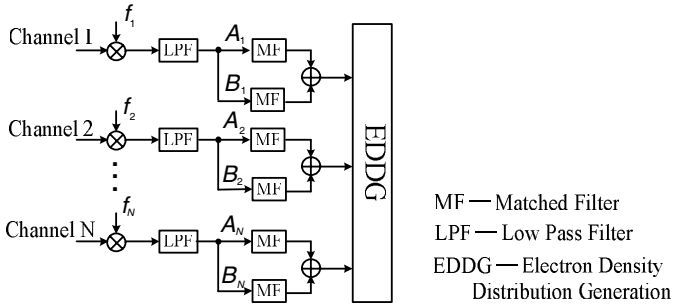

(b)

Figure 2. FDCD MIMO radar system model. (a) Transmitting model. (b) Receiving model.

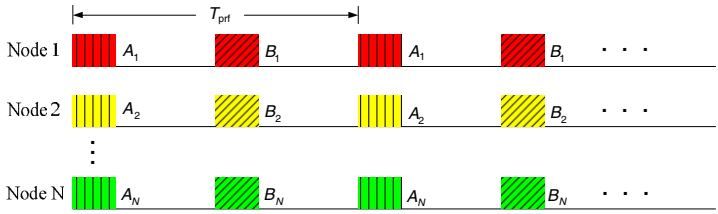

Figure 3. The waveforms of node $1, 2, \ldots, N$.

Figure 2 illustrates the FDCD MIMO radar system. CC-S generator simultaneously generates N pairs of CC-Ss with the repetition period of T_p. B_i, $i = 1 \ldots N$, is delayed by one pulse period that is half T_p through pulse period delayer. Figure 3 shows the waveforms of each node in Figure 2. Then A_i and B_i are modulated by frequency f_i and transmitted alternately. N pairs of CC-S pulses $\{A_i, B_i\}$ with individual frequencies f_i are transmitted simultaneously.

In each receiving channel, the echo signal (consisting of sub-echoes at N frequencies) is mixed by the corresponding carrier frequency f_i, before passing through low pass filter (LPF) to yield the baseband echo signal. Afterwards, the complementary echo signal pair corresponding to $\{A_i, B_i\}$ is compressed by means of matched filtering and superposition (see (10)). Consequently, the delay time t_i can be directly detected from the compressed signal to derive the virtual range. (4) and (8) are used to inverse the one-dimensional electron density profile as function of the true height.

Consequently, two-dimensional electron density profile can be derived by combining the one-dimensional profiles obtained in each repetition period of CC-S pair pulses. It means the image of electron density distribution can be generated as function of true height and azimuth position, and the azimuth resolution can be given as V_s/f_{prf}, where V_s denotes satellite velocity and f_{prf} is repetition frequency of CC-S pair pulses, i.e., $f_{prf} = 1/T_p$.

4. SYSTEM PARAMETERS DESIGN

According to previous and current topside ionosphere sounders that were successfully launched into space, e.g., TOPAS etc., the typical swept-frequency lies within the range of 0.1 MHz–15 MHz ($f_{\min} = 0.1$ MHz and $f_{\max} = 15$ MHz). The plasma frequency f_v at the satellite height and maximum plasma frequency f_m at the lower boundary of topside ionosphere is chosen as the frequency of the first and last echo respectively, corresponding to the minimum and maximum frequency of echoes respectively. Thus, the maximum error of f_v and

f_m relative to true frequency equals to the transmitting frequency interval Δ. According to [21], the number of CC-S pairs N equals to 2^n $(n = 1, 2, \ldots)$. To reduce the scaling error of f_v and f_m, N is chosen as 256, then the frequency interval $\Delta = 0.058\,\text{MHz}$ and the maximum error of f_v and f_m is 0.058 MHz, which is appropriate validated by simulation results in Section 5. The sequence length L is chosen as 1280 [21], leading to pulse compression gain of 2560, (i.e., SNR increased by 34 dB). Therefore, the number of transmitting channels and receiving channels N are 256.

According to the constrain of $f_{\min} = 0.1\,\text{MHz}$, the sub-pulse duration τ is chosen as $10\,\mu\text{s}$. Then the pulse duration $\tau_0 = L \cdot \tau = 12.8\,\text{ms}$.

The satellite height should be higher than the upper boundary of topside ionosphere (about 1000 km) [22]. Assume $H_s = 1100\,\text{km}$. The semi-major is approximately 7471.14 km. According to (12), the satellite velocity is approximately 7.3 km/s.

$$V_s = a \cdot \omega = \sqrt{\frac{\mu}{a}} \tag{12}$$

where a and ω denote the semi-major axis and the average angular velocity of the satellite, respectively, and μ is gravitation constant.

The repetition frequency of radar f_{prf} should satisfy following equation

$$\frac{1}{2f_{prf}} > \tau_0 + t_{\max} \tag{13}$$

where τ_0 is the pulse duration, $t_{\max}$ is the maximum delay time, which is the delay time of signal from lower boundary of topside ionosphere. In practice, the electron density varies with time and location, thus $t_{\max}$ is unknown value. The Chapman model for the depletion of electron density was employed to calculate a typical value of $t_{\max}$ for preliminary system design, shown in (14).

$$N_e(h) = N_0 \exp\left\{0.5\left[1 - \frac{h - h_0}{H} - \exp\left(-\frac{h - h_0}{H}\right)\right]\right\} \tag{14}$$

where N_0 denotes the peak electron density, h_0 is the height where the electron density reaches N_0, H is a scale height. Typical parameters in (14) are chosen as $N_0 = 1 \times 10^{12}\,\text{m}^{-3}$, $h_0 = 350\,\text{km}$, $H = 50\,\text{km}$ [23]. Considering $r = H_s - h$, substituting (14) for $N_e(r)$ in (3), the virtual range corresponding to h_0 is 1935 km through integration, and the corresponding $t_{\max}$ is 0.0129 s. Then according to (13), f_{prf} should be smaller than 19.5 Hz. Taking into consideration, the uncertainty of $t_{\max}$, f_{prf} is selected as 15 Hz.

According to the above mentioned V_s and f_{prf}, the azimuth resolution of the novel topside ionosphere sounder is as high as 0.49 km, which is 153 times higher than TOPAS. Therefore, it is straightforward that the novel FDCD MIMO radar system is more efficient than current topside ionosphere sounders.

5. SIMULATION AND DISCUSSIONS

An assumed ionosphere scenario is employed in the simulation. By assuming that ionospheric electron density distribution satisfies the model of an irregular structure superimposed on the background electron density, it is given by [17]:

$$N_e(h,x) = N(h) \cdot F(x,h) \tag{15}$$

where h and x denote height and azimuth range, $N(h)$ is the background electron density and it is assumed to satisfy IRI2007 model, and $F(x,h)$ is a function for the depletion of an ionospheric irregular electron density structure as [17]:

$$F(x,h) = 1 + A \cdot f(x) \cdot f(h) \tag{16}$$

$$f(x) = \left(1 + \exp\left[-\frac{x - x_1}{a_1}\right]\right)^{-1} - \left(1 + \exp\left[-\frac{x - x_2}{a_2}\right]\right)^{-1} \tag{17}$$

$$f(h) = \left(1 + \exp\left[-\frac{h - h_1}{b_1}\right]\right)^{-1} - \left(1 + \exp\left[-\frac{h - h_2}{b_2}\right]\right)^{-1} \tag{18}$$

where A is a constant, which is negative for the depletion of a ionospheric bubble structure. The bubble is an attenuation part of electron density relative to calm background ionosphere. x_1, x_2, h_1, h_2 denote the positions of the boundaries of the irregular structure, and a_1, a_2, b_1, b_2 denote the thicknesses of boundaries.

According to the radar system parameters designed in part IV and the ionosphere parameters shown in Tables 1 and 2, the system scheme

Table 1. IRI2007 parameters.

Parameters	Year	Month	Day	Lon.	Lat.	UT
Values	2003	1	1	0°	0°	1.5

Table 2. Bubble parameters.

Parameters	A	x_1	x_2	a_1	a_2	h_1	h_2	b_1	b_2
Values/km	−1	15	35	0.3	0.3	100	420	50	50

was validated by simulating radar echoes based on Equations (3) and (15).

Figure 4 is the assumed topside electron density distribution directly generated by (15). There is a bubble irregularity stretched along azimuth position, i.e., 15 km $\leq x \leq$ 35 km. Considering the boundary thickness, the upper boundary of the bubble is height 450 km which is the peak electron density height. An eighth-degree polynomial is used for inversion given in (4). The two-dimensional electron density image is shown in Figure 5, in which the one-dimensional electron density profiles at $x = 0$ km and $x = 25$ km is shown in Figures 6 and 7 respectively. In Figure 5 the empty part is the bubble irregularity, for the electron densities corresponding to frequencies larger than the maximum frequency can not be inversed. It can be seen that there is small empty part along horizontal axis x at the bottom of the image in Figure 5, which means that the maximum electron densities along horizontal axis x can not be inversed due to error in f_m. In simulation, the maximum error of f_m along x is 0.0578 MHz, which occurs at the

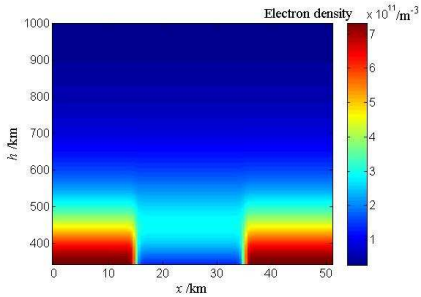

Figure 4. Electron density distribution model.

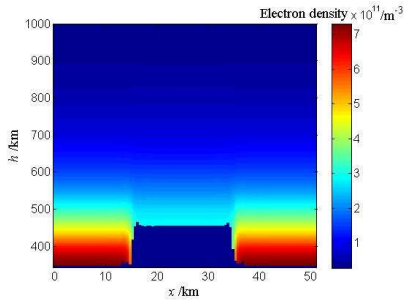

Figure 5. Two-dimensional image simulation result.

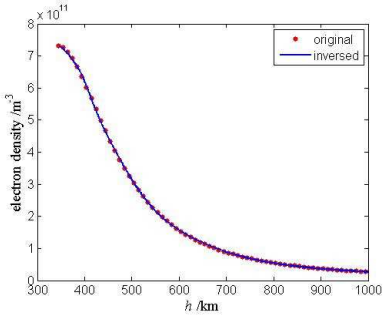

Figure 6. One-dimensional profile at $x = 0$ km.

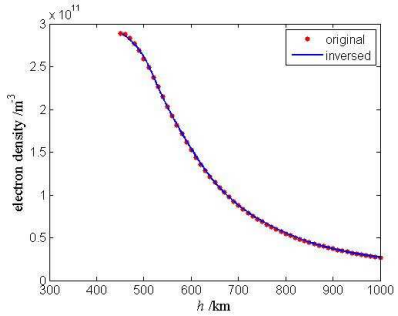

Figure 7. One-dimensional profile at $x = 25$ km.

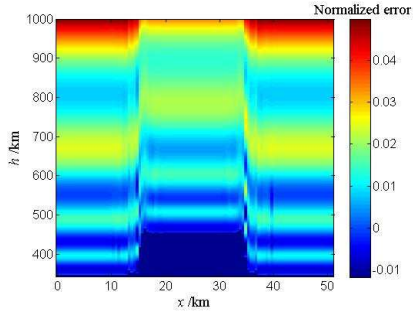

Figure 8. Normalized error of electron density.

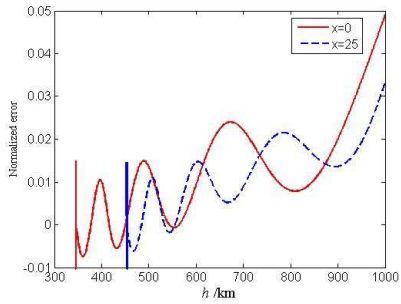

Figure 9. Normalized error at $x = 0$ km and $x = 25$ km.

upper boundary of the bubble irregularity and the height error is about 5 km. Figure 8 shows the normalized electron density measurements error (corresponding to Figure 5) between inversion result N_{inv} and original distribution N_{ori}, given as $(N_{inv} - N_{ori})/N_{ori}$, in which the one-dimensional result at $x = 0$ km and $x = 25$ km is shown in Figure 9. The normalized error is caused by the error of f_v and polynomial fit error. In simulation, the error of f_v is 0.0487 MHz, which is close to the maximum scaling error, and the RMS of normalized electron density measurements error in Figure 8 is only 1.7%, which is acceptable.

The results validate the effectiveness of the proposed system. The system can acquire a two-dimensional electron density image with a high azimuth resolution, which can not be achieved with the current ionosphere models.

6. CONCLUSIONS

Based on multiple channels for transmission and reception, a novel strategy for topside ionosphere sounder based on spaceborne MIMO radar with FDCD is proposed, which can generate two-dimensional electron density image. Both acquisition efficiency and azimuth resolution of the innovative topside ionosphere sounder are significantly improved by using FDCD technique. The azimuth resolution is improved by 153 times compared with TOPAS. This can complement the Total Electron Content (TEC) and electron density data of current models and benefit the detection of topside ionosphere irregularities at scales in km. The proposed system scheme is simulated using IRI2007 model, and the simulation results show the RMS of normalized electron density measurements error is as low as 1.7%, which validates the feasibility and effectiveness of system scheme.

The increased complexity and weight of the system caused by applying multiple channels can be effectively mitigated by employing software defined radio transceiver [4, 24]. Future work will be concentrated on consummating detailed system scheme.

ACKNOWLEDGMENT

The authors would like to thank the reviewers for their perceptive comments and suggestions, which significantly helped us to improve the paper. This work described in the paper was supported in part by the National Natural Science Foundation of China (NSFC) under Grant 60602045 and in part by the Fundamental Research Funds for the Central Universities, China under Grant YWF-10-01-A24.

REFERENCES

1. Chen, J., S. Quegan, and X. Yin, "Calibration of spaceborne linearly polarized low frequency SAR using polarimetric selective radar calibrators," *Progress In Electromagnetics Research*, Vol. 114, 89–111, 2011.
2. Chaudhary, K. and B. R. Vishvakarma, "Effect of ionospheric induced depolarization on satellite solar power station," *Progress In Electromagnetics Research Letters*, Vol. 9, 39–47, 2009.
3. Wu, M., B. Y. Wen, and H. Zhou, "Ionospheric clutter suppression in HF surface wave radar," *Journal of Electromagnetic Waves and Applications*, Vol. 23, No. 10, 1265–1272, 2009.
4. Ganguly, S., V. Wickwar, and J. M. Goodman, "New generation topside sounder," *Radio Science*, Vol. 36, No. 5, 1167–1180, 2001.
5. Reinisch, B. W., D. M. Haines, R. F. Benson, et al., "Radio sounding in space: Magnetosphere and topside ionosphere," *Journal of Atmospheric and Solar-Terrestrial Physics*, Vol. 63, No. 2, 87–98, 2001.
6. Keowsawat, P., C. Phongcharoenpanich, S. Kosulvit, J. Takada, and M. Krairiksh, "Mutual information of MIMO system in a corridor environment based on double directional channel measurement," *Journal of Electromagnetic Waves and Applications*, Vol. 23, Nos. 8–9, 1221–1233, 2009.
7. Golparvar Roozbahani, M. G., E. Jedari, and A. A. Shishegar, "A new link-level simulation procedure of wideband MIMO radio channel for performance evaluation of indoor WLANs," *Progress In Electromagnetics Research*, Vol. 83, 13–24, 2008.

8. Lee, H.-H., J.-H. Lee, H.-K. Song, and C.-K. Song, "Simple and efficient received signal detection technique using channel information for MIMO-OFDM," *Journal of Electromagnetic Waves and Applications*, Vol. 23, Nos. 11–12, 1417–1428, 2009.
9. You, Y.-H. and J. B. Kim, "Pilot and data symbol-aided frequency estimation for UWB-OFDM," *Progress In Electromagnetics Research*, Vol. 90, 205–217, 2009.
10. Wang, Y. and H. Li, "A novel antenna selection scheme for amplify-and-forward MIMO relay systems," *Journal of Electromagnetic Waves and Applications*, Vol. 24, No. 11–12, 1531–1543, 2010.
11. Fishler, E., A. Haimovich, R. S. Blum, et al., "Spatial diversity in radars-models and detection performance," *IEEE Trans. on Signal Processing*, Vol. 54, No. 3, 823–838, 2006.
12. Qu, Y., G. Liao, S.-Q. Zhu, X.-Y. Liu, and H. Jiang, "Performance analysis of beamforming for MIMO radar," *Progress In Electromagnetics Research*, Vol. 84, 123–134, 2008.
13. Wang, G. and Y.-L. Lu, "Sparse frequency waveform design for MIMO radar," *Progress In Electromagnetics Research B*, Vol. 20, 19–32, 2010.
14. Huang, Y., P. V. Brennan, D. Patrick, I. Weller, P. Roberts, and K. Hughes, "FMCW based MIMO imaging radar for maritime navigation," *Progress In Electromagnetics Research*, Vol. 115, 327–342, 2011.
15. Helliwell, R. A., *Whistlers and Related Ionospheric Phenomena*, *Dover Publicaions*, Mineola, New York, 2006.
16. Yesil, A., M. Aydogdu, and A. G. Elias, "Reflection and transmission in the ionosphere considering collisions in a first approximation," *Progress In Electromagnetics Research Letters*, Vol. 1, 93–99, 2008.
17. Zernov, N. N., V. E. Gherm, and H. J. Strangeways, "On the effects of scintillation of low-latitude bubbles on transionospheric paths of propagation," *Radio Science*, Vol. 44, RS0A14, 1–9, 2009.
18. Sadighi, S., P. T. Jayachandran, et al., "Comparison of the CHAMP radio occultation data with the Canadian advanced digital ionosonde in the Polar Regions," *Advances in Space Research*, Vol. 44, No. 11, 1304–1308, 2009.
19. Li, S. F., J. Chen, and L. Q. Zhang, "Optimisation of complete complementary codes in MIMO radar system," *Electronics Letters*, Vol. 46, No. 16, 1157–1158, 2010.
20. Li, S., J. Chen, L. Zhang, and Y.-Q. Zhou, "Application of

complete complementary sequence in orthogonal MIMO SAR system," *Progress In Electromagnetics Research C*, Vol. 13, 51–66, 2010.

21. Li, S. F., J. Chen, L. Q. Zhang, et al., "Construction of quadriphase complete complementary pairs applied in MIMO radar systems," *ICSP2008 Proceedings*, 2298–2301, 2008.
22. Carpenter, D. L., "Remote sensing the earth's plasmasphere," *Radio Science Bulletin*, Vol. 308, 13–29, 2004.
23. Liu, J., Y. Kuga, et al., "Ionospheric effects on SAR imaging: A numerical study," *IEEE Trans. Geosci. Remote Sens.*, Vol. 41, No. 5, 939–947, 2003.
24. De La Morena-Álvarez-Palencia, C. and M. Burgos-Garcia, "Four-octave six-port receiver and its calibration for broadband communications and software defined radios," *Progress In Electromagnetics Research*, Vol. 116, 1–21, 2011.